Categorization of Mineral Resources Based on Different Geostatistical Simulation Algorithms: A Case Study from an Iron Ore Deposit

Nurassyl Battalgazy & Nasser Madani

Natural Resources Research

ISSN 1520-7439

Nat Resour Res
DOI 10.1007/s11053-019-09474-9

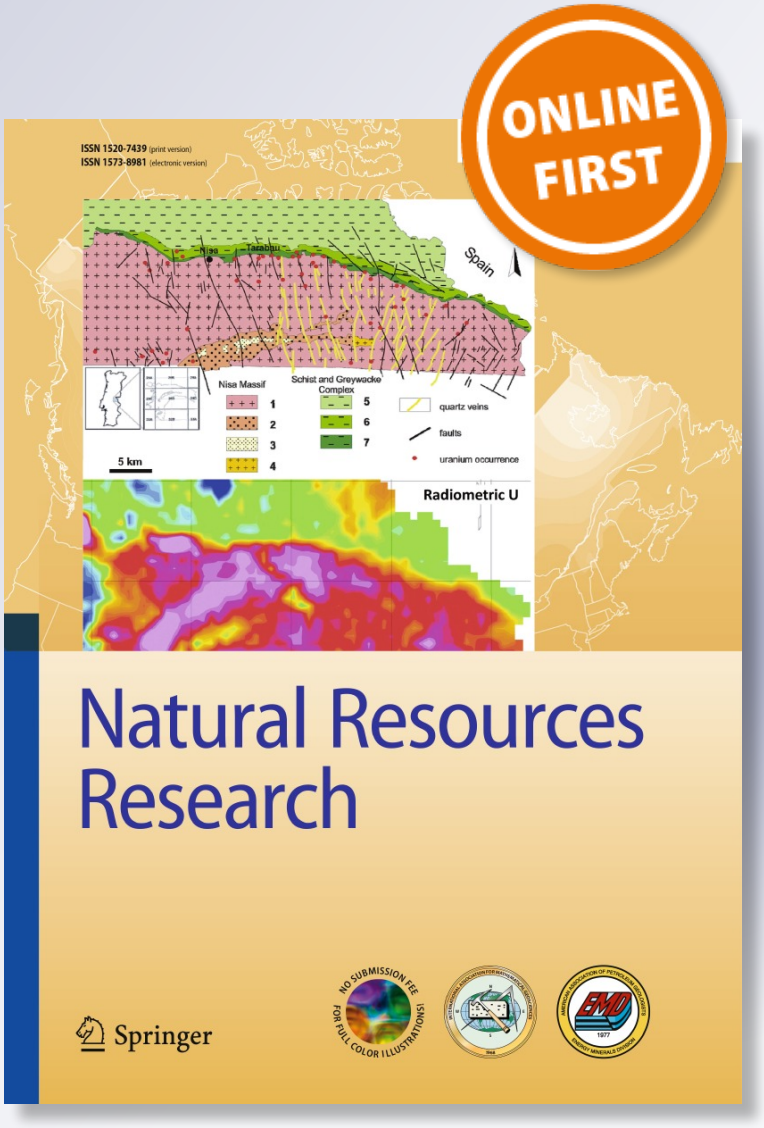

Springer

Natural Resources Research (© 2019)
https://doi.org/10.1007/s11053-019-09474-9

Original Paper

Categorization of Mineral Resources Based on Different Geostatistical Simulation Algorithms: A Case Study from an Iron Ore Deposit

Nurassyl Battalgazy[1] and Nasser Madani[1,2]

Received 24 November 2018; accepted 4 March 2019

Mineral resource classification plays an important role in the downstream activities of a mining project. Spatial modeling of the grade variability in a deposit directly impacts the evaluation of recovery functions, such as the tonnage, metal quantity and mean grade above cutoffs. The use of geostatistical simulations for this purpose is becoming popular among practitioners because they produce statistical parameters of the sample dataset in cases of global distribution (e.g., histograms) and local distribution (e.g., variograms). Conditional simulations can also be assessed to quantify the uncertainty within the blocks. In this sense, mineral resource classification based on obtained realizations leads to the likely computation of reliable recovery functions, showing the worst and best scenarios. However, applying the proper geostatistical (co)-simulation algorithms is critical in the case of modeling variables with strong cross-correlation structures. In this context, enhanced approaches such as projection pursuit multivariate transforms (PPMTs) are highly desirable. In this paper, the mineral resources in an iron ore deposit are computed and categorized employing the PPMT method, and then, the outputs are compared with conventional (co)-simulation methods for the reproduction of statistical parameters and for the calculation of tonnage at different levels of cutoff grades. The results show that the PPMT outperforms conventional (co)-simulation approaches not only in terms of local and global cross-correlation reproductions between two underlying grades (Fe and Al_2O_3) in this iron deposit but also in terms of mineral resource categories according to the Joint Ore Reserves Committee standard.

KEY WORDS: Mineral resource classification, Projection pursuit multivariate transform, Joint simulation, Iron deposit, JORC code.

INTRODUCTION

Mineral resource estimation is a classification of deposits to measured, indicated and inferred based upon qualified degrees of geological confidence. This estimation indicates a prominent requirement for public reporting and internal company assessments, financial institutions and authorities, investors, environmental risk evaluation, professional advisors, stock exchanges and government agencies (Vallée 1999, 2000; Snowden 2001; Dohm 2005; Dimitrakopoulos et al. 2009; Rossi and Deutsch 2014; Silva and Boisvert 2014; Krzemień et al. 2016; Fox 2017; Menin et al. 2017). Different classification standards have been developed in some countries, mostly similar in purpose and template. The main widely used standards are from the Joint Ore Re-

[1]School of Mining and Geosciences, Nazarbayev University, Astana, Kazakhstan 010000.
[2]To whom correspondence should be addressed; e-mail: nasser.madani@nu.edu.kz

Published online: 11 March 2019

serves Committee (JORC, www.jorc.org) in Australia; the Canadian Institute of Mining (CIM) guidelines (NI 43-101) in Canada (www.cim.org); the South African Code for the Reporting of Exploration Results, Mineral Resources and Mineral Reserves, i.e., the SAMREC code in South Africa (www.saimm.co.za/samrec.asp) and the Pan-European Union and United Kingdom's Reporting Code (www.crirsco.com/PERC_REPORTING_CODE_jan2009.pdf). Among others, the JORC code seems popular with wider acceptance. Although those codes are important guidelines, they do not provide a straightforward technique for resource classification (Rossi and Deutsch 2014). The categorization of mineral resources in the JORC standard generally depends on the geological model of the deposit, the sampling quality and the data spacing (Silva and Boisvert 2014; Rivoirard and Renard 2016). Based on JORC code, "**Measured Mineral Resource** is a subpart of the Mineral Resource in which the estimation of the grade, quantity, density, shape and physical characteristics are based on the evidence from reliable and detailed exploration results, sampling, testing collected from drill holes, trenches, pits and outcrops. The Measured Mineral Resource has the highest level of confidence among other parts and can be altered to a Proved Ore Reserve. Thus, Measured Mineral Resource can be applied for risk analysis, detailed mine planning and final assessment of economic viability of the mine project," "**Indicated Mineral Resource** is a subpart of the Mineral Resource in which the estimation of the grade, quantity, density, shape and physical characteristics are based on the geologic pieces of evidence from proper exploration results, sampling, testing collected from drill holes, pits and outcrops. The Indicated Mineral resource has a higher level of confidence than Inferred Mineral Resource and thus can be used for further analysis of mine planning and assessment of economic viability of the mine project." "**Inferred Mineral Resource** is a subpart of the Mineral Resource in which the estimation of grade and quantity is based on the sampling and limited geological evidence. The Inferred Mineral Resource has the lowest level of confidence and thus cannot be altered to an Ore Reserve."

The techniques of resource categorizations can be classified into two main families. The first family, the deterministic approach, relates to block-by-block identification of confidence intervals through either geometric or geostatistical schemes. In a geometric scheme (e.g., drill hole spacing and neighborhood restriction), confidence in the estimated block highly relies on data spacing or proximity between sample points (Deutsch et al. 2006; Emery et al. 2006; Naus 2008; Wilde 2010). In this approach, however, data redundancy is neglected and spatial continuity may not be considered (Rivoirard and Renard 2016). In a geostatistical scheme, the estimation outputs (e.g., kriging variance) play an important role, respecting spatial continuity as it is significantly considered in the computation (Krige 1996, 1999; Arik 1999, 2002; Yamamoto 2000; Mwasinga 2001; Sinclair and Blackwell 2002). Nevertheless, the smoothing effect of the conditional distribution and ignoring the proportional effect in the kriging system imposes difficulties in interpreting the kriging variance for mineral resource classification (Dimitrakopoulos et al. 2009; Rossi and Deutsch 2014; Silva and Boisvert 2014). An alternative for obtaining more trustworthy results is the second family, namely stochastic simulations, the uncertainty for which can be explicitly quantified at the block locations (Snowden 2001; Dominy et al. 2002; Dohm 2005; Wawruch and Betzhold 2005; Deutsch et al. 2006; Emery et al. 2006; Manchuk et al. 2009). Conditional simulations provide realizations with true grade variability and are capable of computing the uncertainty in a global and local sense in the total amount of resources at different thresholds and cutoff grades. Although there are some legitimate criticisms regarding uncertainty models derived from conditional simulations for resource classification (Deutsch et al. 2006), due to its dependency on the implementation parameters employed in a simulation (Rossi 2003), this approach still presents greater tractability, depending on the choice of the geostatistical simulation algorithm and the accurate setting of its relevant parameters (Murphy et al. 2004; Duggan and Dimitrakopoulos 2005; Emery et al. 2006; Sadeghi et al. 2015). Regarding this issue, many approaches have been proposed and developed to improve stochastic 3D spatial modeling of regionalized variables. For cross-correlated variables, co-simulation approaches are highly advocated over independent simulation approaches because the spatial cross-dependency can be taken into account (Wackernagel 2003; Chilès and Delfiner 2012; Paravarzar et al. 2015; Madani and Ortiz 2017; Eze et al. 2019; Abildin et al. 2019). In some special circumstances, for example, the variables behave differently and show some complex interrelationship characteristics, and

the use of conventional approaches is restricted (Boisvert et al. 2013; Deutsch 2013). To address this problem, enhanced co-simulation algorithms based on factorization techniques have been developed (Leuangthong and Deutsch 2003; Barnett et al. 2014). Among others, the projection pursuit multivariate transform (PPMT) (Barnett et al. 2014, 2016) is an approach that can handle any complexity that exists among the variables (Barnett et al. 2014, 2016; Hosseini and Asghari 2018).

The objectives of this paper are fourfold: (1) briefly present the conventional (co)-simulation approaches and the PPMT (in this study, the turning bands (co)-simulation (Emery and Lantuéjoul 2006; Emery 2008) is opted for the conventional approach); (2) describe the application of these approaches in a real case study for an iron deposit in Brazil; (3) describe the stochastic classification of mineral resources based on the output derived from objective #2 and compare them in terms of a tonnage evaluation; and (4) discuss the pros and cons of mentioned methods.

METHODS

Turning Bands (co)-Simulation

A turning bands simulation is an approximate algorithm based on multi-Gaussianity assumption of an underlying random field. This algorithm was first introduced by Matheron (1973) and then extended in some organized program codes by Lantuéjoul (1994) and Emery and Lantuéjoul (2006). The principal concept of this algorithm is based on firstly, drawing numerous randomly orientated lines and secondly, simulating a one-dimensional Gaussian random field along each line (Lantuéjoul 1994, 2002). In other words, the core of the turning bands algorithm is to simplify the simulation problem in R^3 or R^2 into a R problem. The random field $\{Y(x), x \in R^d\}$ is defined in Eq. 1 with a zero mean and isotropic covariance C_Y (Eq. 2), where U is a uniform distribution over S_d, which is the unit sphere of R^d.

$$Y(x) = X(\langle x, U\rangle) \text{ for any location of } \forall x \in R^\mathrm{d} \quad (1)$$

$$C_Y(r) = \int_{S_\mathrm{d}}^{N} C_X(\langle h, u\rangle)\omega_\mathrm{d}(\mathrm{d}u) \quad (2)$$

where $<$ and $>$ are the inner standard products in R^d, h is a vector of R^d, u is a unit vector of R^d, ω_d is a uniform distribution over S_d and r is the modulus of R^d.

As mentioned above, Matheron (1973) first introduced and proved the relationship (Eq. 2) between continuous and isotropic covariances in R^d with continuous covariances in R. By using this algorithm, one can substitute a multi-dimensional simulation with a one-dimensional simulation.

Having the covariance model fitted to the primary declustered normal score variable, the covariance function is derived in one-dimensional random fields. The turning bands simulation provides a non-conditional multi-dimensional random field compatible with the target covariance model, in which the simulated values are practically standard Gaussian (Emery and Lantuéjoul 2006). To generate the conditional realizations, the non-conditional simulation obtained should be progressed through the postprocessing of the kriging step (Journel and Huijbregts 1978; Emery 2008; Chilès and Delfiner 2012).

In the turning bands co-simulation approach, it is of interest to stochastically simulate cross-correlated variables (e.g., more than two). In this case, the cross-covariance function is needed to be constructed taking into account the transformed variables in the sample points with multi-dimensional Gaussian random fields. The non-conditional step is the same as turning bands simulation for each variable; however, in part of the conditioning mechanism, the co-kriging method must be used rather than the kriging method to hold the multivariate characteristics (Carr and Myers 1985; Myers 1989; Gutjahr et al. 1997; Emery 2008):

$$Y_{CCS}(x) = Y^{\mathrm{SCK}}(x) + \left[Y_S(x) - Y_S^{\mathrm{SCK}}(x)\right] \quad (3)$$

where $Y^{\mathrm{SCK}}(x)$ is simple co-kriging of $Y(x)$ from conditioning data, $Y_S(x)$ is non-conditional simulation at location x for the variables; $Y_S^{\mathrm{SCK}}(x)$ is a simple co-kriging system for the non-conditional simulation from its value at the data locations. This simple co-kriging system can also be substituted for an ordinary co-kriging paradigm (Emery 2007).

The general workflow in the turning bands co-simulation is similar to the previously explained turning bands simulation; however, in the variogram analysis, because the co-kriging system is established on the basis of the cross-covariance matrix, it is

necessary to calculate the direct and cross-variograms. To fit the theoretical direct and cross-variogram models, as an alternative, a linear model of co-regionalization (LMC) can be used to fit all experimental variograms as a linear combination of the equivalent structures together with the identical ranges but different sills (Wackernagel 2003; Chilès and Delfiner 2012). The most tedious part of this job is to construct the permissible positive semi-definiteness conditions for fitting the sill matrices. Once this constraint is corroborated, the model can be used in the variance–covariance matrix required in the conditioning process (Goovaerts 1997).

Multi-Gaussian Transformation

Because the turning bands (co)-simulation algorithm is based on the multi-Gaussianity assumption of input data, variables should be transformed to standard Gaussian model with a mean of 0 and a variance of 1. The step can be performed through Gaussian anamorphosis (Rivoirard 1994) or a quantile-based approach (Deutsch and Journel 1998). In multivariate cases, it is a common practice to transfer each variable separately to a normal standard score and employ one of the widespread functions of the Gaussian (co)-simulation. The most important aspect of this approach in the case of the existence of complexities among bivariate relations of variables is that the multi-Gaussian assumption after transformation may not be valid. Respecting this violation in the multi-Gaussianity assumption, the conventional Gaussian co-simulation algorithms, including turning bands co-simulation, may not be practical. To circumvent this difficulty in such a situation, factor-based approaches based on decorrelation techniques can be applied.

Projection Pursuit Multivariate Transform

One of the newly developed transformation-based approaches is the PPMT method, which is targeted to handle multivariate complexities, such as nonlinearity and heteroscedasticity, which intrinsically exist among the variables (Barnett et al. 2014; Barnett et al. 2016; Barnett 2017). The PPMT is suitable in cases in which the traditional normal standard score transformation does not work properly. The general steps for the implementation of the PPMT are based on forward and backward transformations. Forward transformation converts the original data to an uncorrelated multi-Gaussian distribution, taking into account any type of complexity that exists among the variables, and the simulated results can then be back-transformed to the original scale. This back-transformation is based on the projection pursuit density estimation algorithm (PPDE) (Friedman 1987). Provided that these variables are represented by second-order stationary random fields, the PPMT steps for two variables can be defined as:

1. *Transform the original variables to normal score values with a mean of zero and a variance one* $N(0,1)$. This can be implemented by normal score transformation methodologies such as Gaussian anamorphosis (Rivoirard 1994) or a quantile-based approach (Deutsch and Journel 1998):

$$Z_i(u) = G^{-1}(F_i(Y_i(u))) \quad i = 1,2 \tag{4}$$

where $G^{-1}(.)$ is the standard normal cumulative distribution function, $F_i(.)$ is the cumulative distribution function of the original variables and $Y_i(u)$ and $Z_i(u)$ are normal score values.

2. *Data sphering (A):* Compute the experimental variance–covariance matrix at lag 0. Because we are dealing with normal score values, this matrix is identical to the sample correlation matrix. In the case of two variables, this matrix (V) is:

$$V = \mathrm{Corr}\{Z(u), Z(u)\} = \begin{bmatrix} \rho_{11}(0) & \rho_{12}(0) \\ \rho_{21}(0) & \rho_{22}(0) \end{bmatrix} \tag{5}$$

where the principal diagonal element equals one, which is identical to the total variance and the upper and lower diagonal elements $\rho_{12}(0)$ and $\rho_{21}(0)$ equal the linear correlation coefficient between the two normal score variables $Z_1(u)$ and $Z_2(u)$, respectively.

3. *Data sphering (B):* Perform the spectral decomposition of the above matrix (V) to derive the orthonormal eigenvectors matrix (M_1), associated with the underlying diagonal eigenvalues matrix (E_1), such that:

$$V = M_1 E_1 M_1^T \tag{6}$$

It is necessary to check that the entries of E exhibit a decreasing order.

4. *Data sphering (C)* Calculate the sphering transformations at location u by:

$$\varphi_i(u) = Z_i(u) M_1 E_1^{-1/2} M_1^T \quad i = 1, 2 \tag{7}$$

where $\varphi_i(u)$ are scores with a normal standard distribution due to the priori multivariate Gaussian assumption and are decorrelated.

5. *Projection pursuit* Although the $\varphi_i(u)$ are decorrelated, the complexity still manifests itself in a bivariate relation. Projection pursuit can transform the decorrelated variables $\varphi_i(u)$ to the multi-Gaussian variables free of the underlying complexity. To do so, taking into account that the projection of data is $\tau = \varphi_i(u)\alpha$, where $k * 1$ is a unit vector α, the projection index test statistic is defined as $A(\alpha)$ that determines the univariate non-Gaussianity. When the related projection is appropriately Gaussian, the projection index $A(\alpha) = 0$. According to Friedman (1987), the optimized search is used to determine the θ, which will identify the maximum $A(\alpha)$. The $\varphi_i(u)$ function is transformed to a standard Gaussian, $\varphi_i(u)'$, where the related projection is $\tau' = \varphi_i(u)'\alpha$ after the optimum α is identified. The transformation starts with the application of the Gram-Schmidt algorithm to compute the orthogonal matrix as (Reed and Simon 1972):

$$\omega = [\alpha, \phi_1, \phi_2, \ldots, \phi_{k-1,}] \tag{8}$$

and transformation can be reached by the multiplication of $\varphi_i(u)$ and ω, thus:

$$\varphi_i(u)\omega = [p, \varphi_i(u)\phi_1, \varphi_i(u)\phi_2, \ldots, \varphi_i(u)\phi_{k-1,}] \tag{9}$$

Then, to obtain the transformation that outputs the Gaussian standard projection, τ', the normal score transform is computed, as:

$$\breve{G}(\varphi_i(u)\omega) = [\tau', \varphi_i(u)\phi_1, \varphi_i(u)\phi_2, \ldots, \varphi_i(u)\phi_{k-1,}] \tag{10}$$

and back-transformation to the original basis is computed as:

$$\varphi_i(u) = \breve{G}(\varphi_i(u)\omega)\omega^T \tag{11}$$

The transformed data $\varphi_i(u)'$ outputs the Gaussian projection by α, where the projection index, $A(\alpha)$, is zero. Additionally, to obtain other complexities, an optimized search can be iterated and used to determine the maximum projection index.

6. *Stopping Criteria* This step focuses on the selection of the target projection index. An increase in dimensions leads to the difficult resolution and discovery of complexities, while the number of observations results in the reliability of the projections for the identification of appropriate multivariate structures. Random samples from the Gaussian cumulative density function (CDF) can be used by implementation of a bootstrapping algorithm, where m is the distribution, k is the dimension and n is the number of observations for choosing the target projection index for PPMT stopping. Then, the value of the projection index can be computed.
7. *Back-Transform* Gaussian realizations can then be back-transformed based on the mapped data on an original space, where the configuration between the simulated and mapped data is preserved.

A schematic illustration of the PPMT is provided in Figure 1, which explains how the complexities among the variables can be first decorrelated and then restituted after the process of modeling and backward transformation.

CASE STUDY

Carajas Mine, the study area, which is one of the largest iron ore mines in the world, is located in the Parauapebas municipality, Para state, in northern Brazil. The dataset provided by the Vale Company pertains to iron deposits consisting of iron (Fe) and other trace elements, such as phosphorus (P), manganese (Mn) and aluminum oxide (Al_2O_3). The geological characterization and lithostructural setting of the Carajas Mine are related to the metavolcanic and metasedimentary rocks of the Grao-Para group, which comprises the Parauapebas (Meirelles et al. 1984) and Carajas Formation rocks

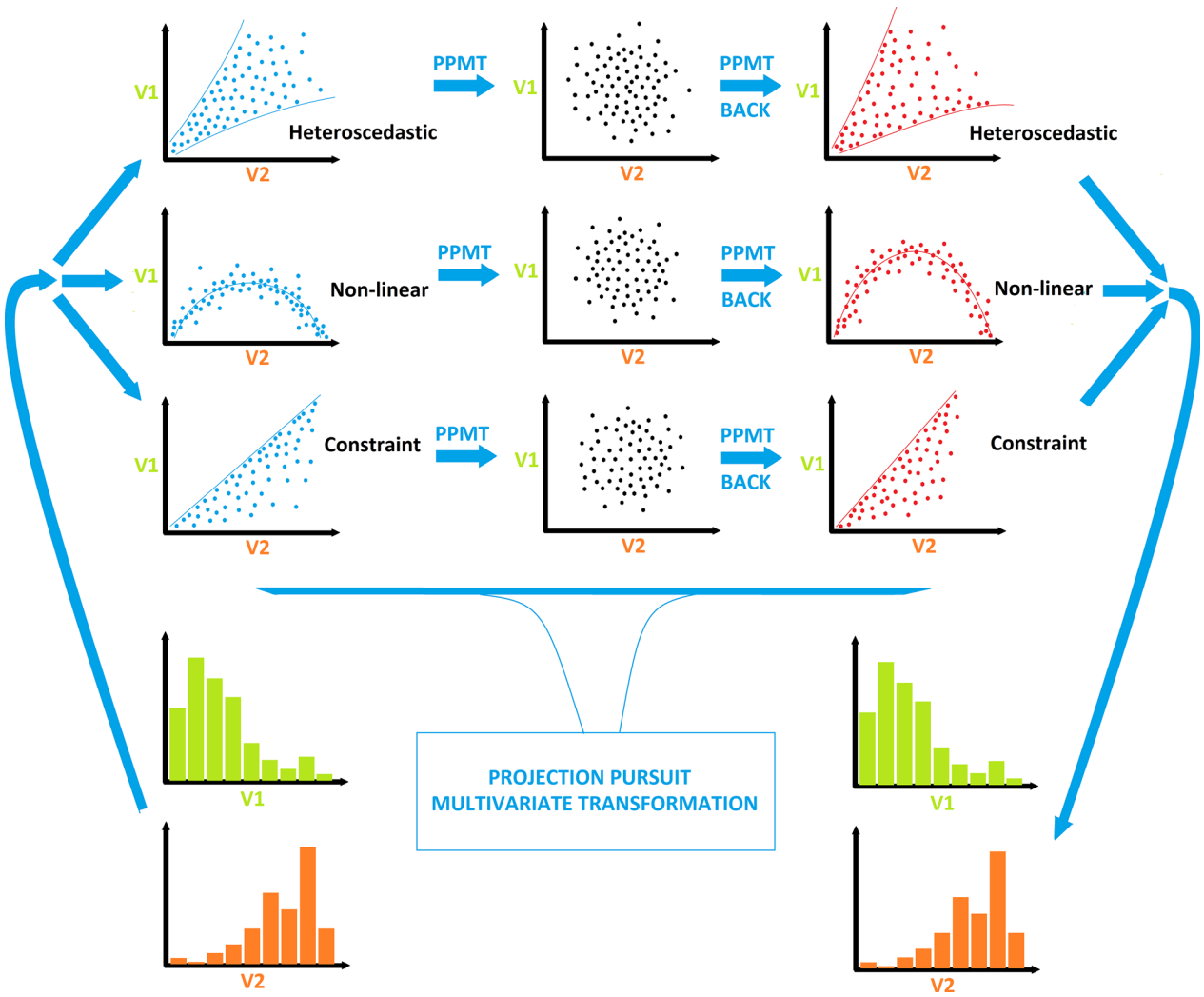

Figure 1. Illustration of projection pursuit multivariate transformation.

(Beisiegel et al. 1973) consisting of volcanic rocks and ironstones, respectively (Fig. 2). The deposits consist mainly of anisotropic and heterogenetic rock masses with different shear strengths. As the deposit are highly concentrated with iron rocks, the lithology includes mainly mafic rocks and ironstones. Mafic rocks are classified with different geotechnical parameters depending on resistance, such as weathered mafic rocks with medium or high resistance and semi-weathered mafic rocks, while the ironstone classification depends on the chemical and physical properties of soft hematite, hard hematite, low content iron ore and jaspelite (Paradella et al. 2015).

Exploratory Data Analysis

The dataset contains 613 samples with isotopic sampling patterns, indicating that all of the variables (Fe and Al_2O_3) are known and share the same location of samples (Wackernagel 2013). The first step in exploratory data analysis includes the detection of all possible outliers and duplicated samples. To recognize the outliers, the possible maximum values are first recognized by typical statistical tools, such as histograms and probability plots (Rossi and Deutsch 2014). Next, the identified extreme values are double checked to ensure that they are valid samples and are not erroneous. Fi-

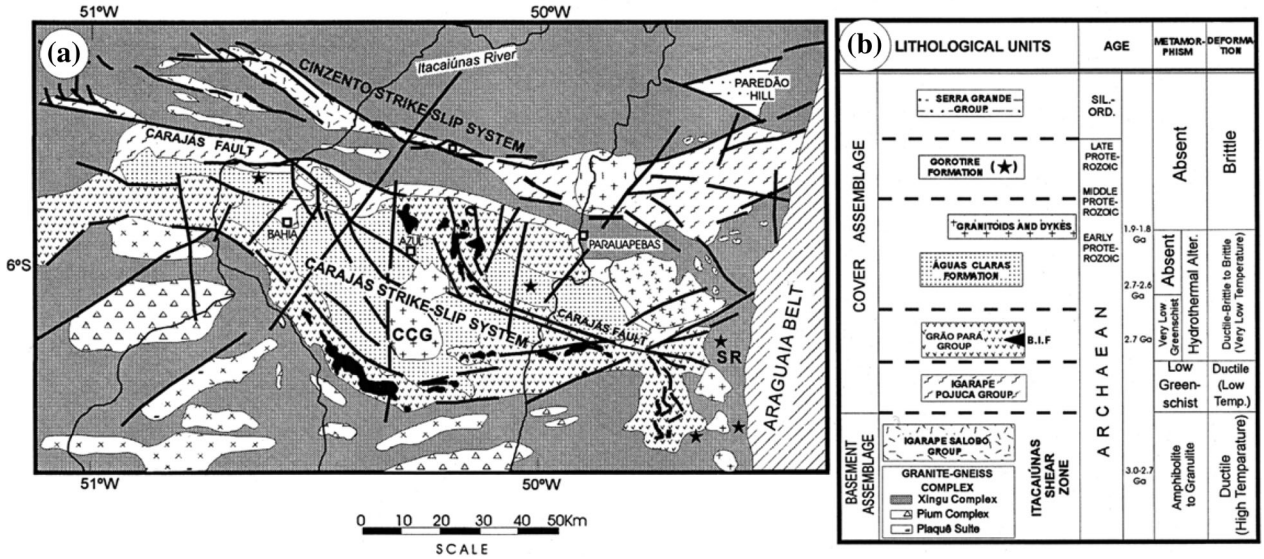

Figure 2. (**a**) Simplified geological map of the Carajas region. (SR = Serra do Rabo region; CCG = central Carajas granite). (**b**) Tectonostratigraphy of the Carajas region (BIF = banded ironstone formation) (Holdsworth and Pinheiro 2000).

nally, those valid values are handled through the capping approach, where values in the upper tail of the distribution could be moved back and reset to the previous maximum values. After this step, the data are declustered to make the global distribution more representative (David 1977; Deutsch 1989). The declustering technique is implemented in a dimension of 800 m × 800 m × 80 m based on the primary pattern of the boreholes. Statistical parameters are then calculated, as shown in Table 1. Declustering ensures that the statistical parameters are representative and that they are no longer impacted by the scarcity of data in some regions. The cell declustering technique (Goovaerts 1997; Deutsch and Journel 1998) is applied in this study to correct the pseudo-skewness in the global distribution of Fe and Al_2O_3. In this method, the area of interest should first be divided into a grid of cells, and weights are then assigned to each data value according to the number of samples falling in the same cell. The resulting weights in the occupied cells are greater than zero and in total sum to one, while vacant cells receive no weight (Rossi and Deutsch 2014; and references herein).

Figure 3 shows the dependency of the covariables and the correlation coefficient between declustered Fe and Al_2O_3. The computed correlation coefficient (− 0.82) shows that two variables are highly correlated. The negative sign also corroborates that the global variability of Fe in the region is highly controlled by Al_2O_3; thus, an increase in the Fe grade in the region corresponds to a decrease in the amount of Al_2O_3. This type of good correlation advocates the use of co-simulation methods rather than independent simulation methods because co-simulation takes into account the intrinsic correlation between covariables (Eze et al. 2019; Abildin et al. 2019).

As explained earlier, the scope of this research is to jointly model Fe and Al_2O_3, taking into account the correlation coefficient between them and to reproduce the bivariate relation shape, as illustrated in Figure 3. Technically, the characteristics of the bivariate relation reveal that the lower quantiles of Al_2O_3 are highly dependent on the upper quantiles of Fe (red to green points in the scatterplot), and the linear correlation coefficient is mostly impacted from this range of values. Therefore, this can be interpreted as a complexity in the bivariate relation between Fe and Al_2O_3, and the idea is to reproduce the complexity by restituting the intensity of the correlation beyond the modeling process and then to consider the variation in the mineral resource estimation and reporting based on the JORC code. To do so, the results of two methodologies based on the conventional normal score transformation of variables and the PPMT transformation are compared and discussed.

Table 1. Statistical analysis of Fe and Al_2O_3 in the Carajas deposit

Variables (%)	Number of samples	Minimum	Maximum	Mean	Variance	Correlation
Fe	613	21.2	69.17	63.6	59.94	− 0.82
Al_2O_3	613	0.1	37.2	2.05	19.63	

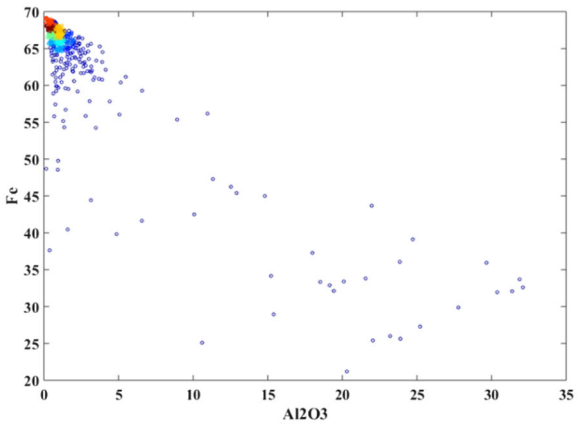

Figure 3. Scatter plot of declustered iron (Fe) and aluminum oxide (Al_2O_3). Correlation coefficient: − 0.82.

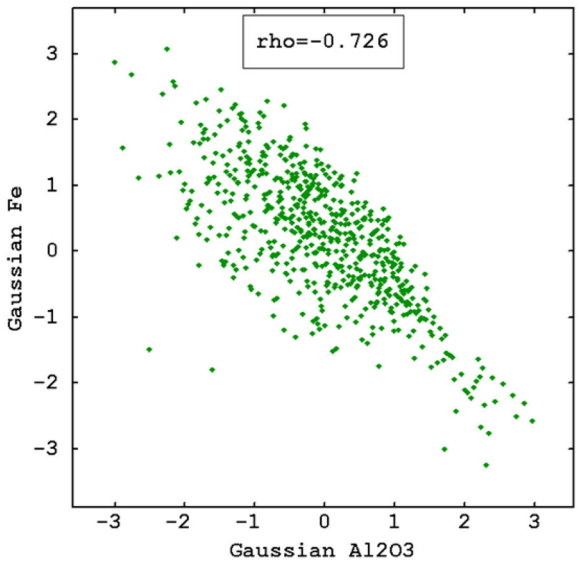

Figure 4. Scatter diagram of Gaussian Al_2O_3 and Fe.

Gaussian Co-simulation Based on the Conventional Normal Score Transformation

The turning bands (co)-simulation approach in this study was applied to the joint simulation of Fe and Al_2O_3 in the Carajas Mine deposit. The first step, after declustering, was to separately transform the variables into normal standards scores (Deutsch and Journel 1998). The step can be performed through either Gaussian anamorphosis (Rivoirard 1994) or a quantile-based approach (Deutsch and Journel 1998). Here, the latter is applied to the dataset because of simplicity and tractability in Gaussian transformation. The scatterplot between normal score variables (Fig. 4) shows that the bivariate multi-Gaussian assumption is somehow respected, indicating approximate elliptical shapes that one expects to see after the transformation. The correlation coefficients also decreased approximately 13% after this normal score transformation. The bivariate multi-Gaussian examination through this figure is only valid at lag zero. The spatial multi-Gaussian assumption can also be separately checked for each transformed variable. This approach is validated by checking their experimental modograms and rodograms (Emery 2005) that are approximately proportional to the square roots of their experimental variograms (Fig. 5).

To implement the turning bands co-simulation method, the direct and cross-variograms of Fe and Al_2O_3 must be quantified over the transformed Gaussian values. The anisotropy is checked by computing the experimental variogram in different directions, and the results showed that one cannot recognize any significant different spatial tendency in experimental variogram characteristics, such as the range (geometric anisotropy) and sill (zonal anisotropy). The variogram map which is a 2D plot of the sample variogram for all experimentally available separation vectors (Deutsch and Journel 1998) is also calculated. Directions of anisotropy are usually evident from a variogram map. However, as can be seen from Figure 6, there is no evidence of different continuities in different directions for the main variable in the case, Fe. Therefore, experimental omnidirectional and cross-variograms are calculated, and a two-structured linear model of the co-regionalizations was fitted. The proper formula is (Fig. 7):

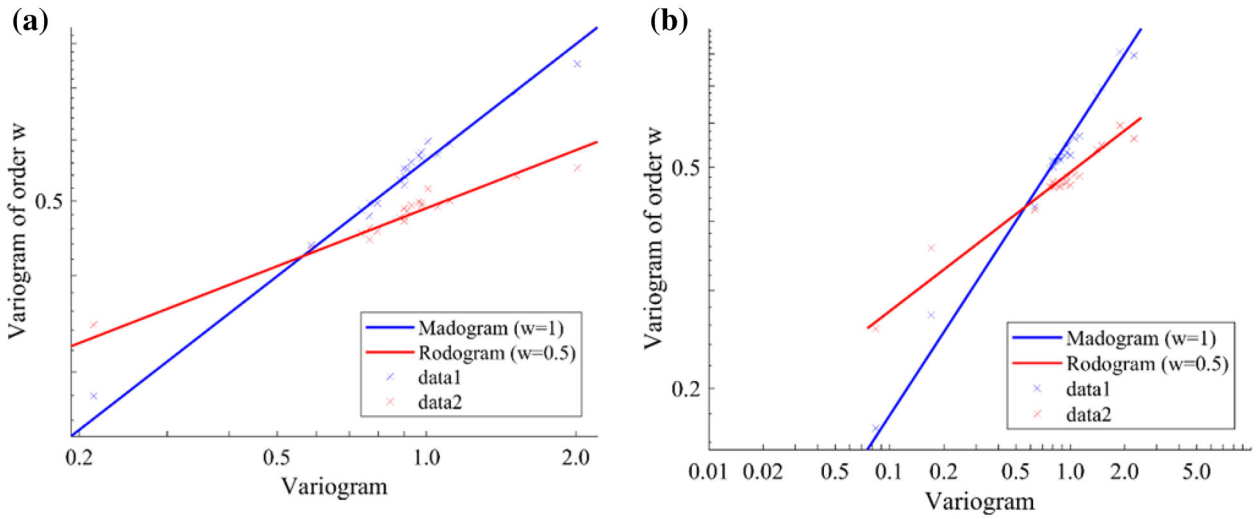

Figure 5. Experimental modograms and rodograms of the Gaussian variables of (**a**) Al_2O_3 and (**b**) Fe as a function of their experimental variograms. In case of multi-Gaussianity assumption, the points should be approximately distributed along the thick solid line.

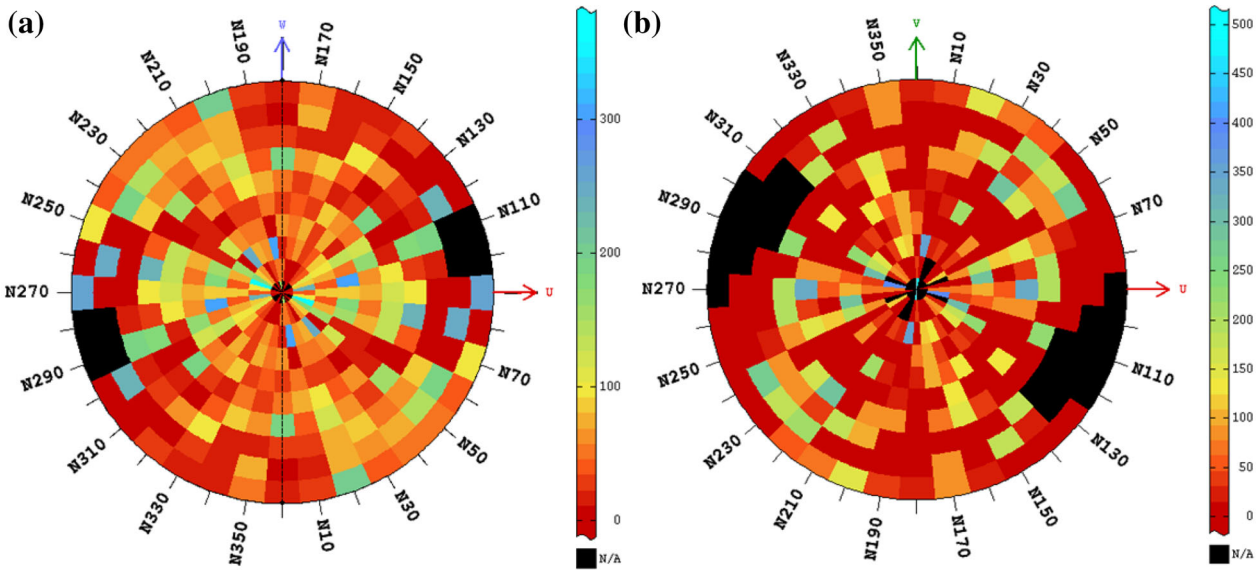

Figure 6. Variogram map in both (**a**) horizontal and (**b**) vertical plans. There is no evidence of anisotropy in both directions.

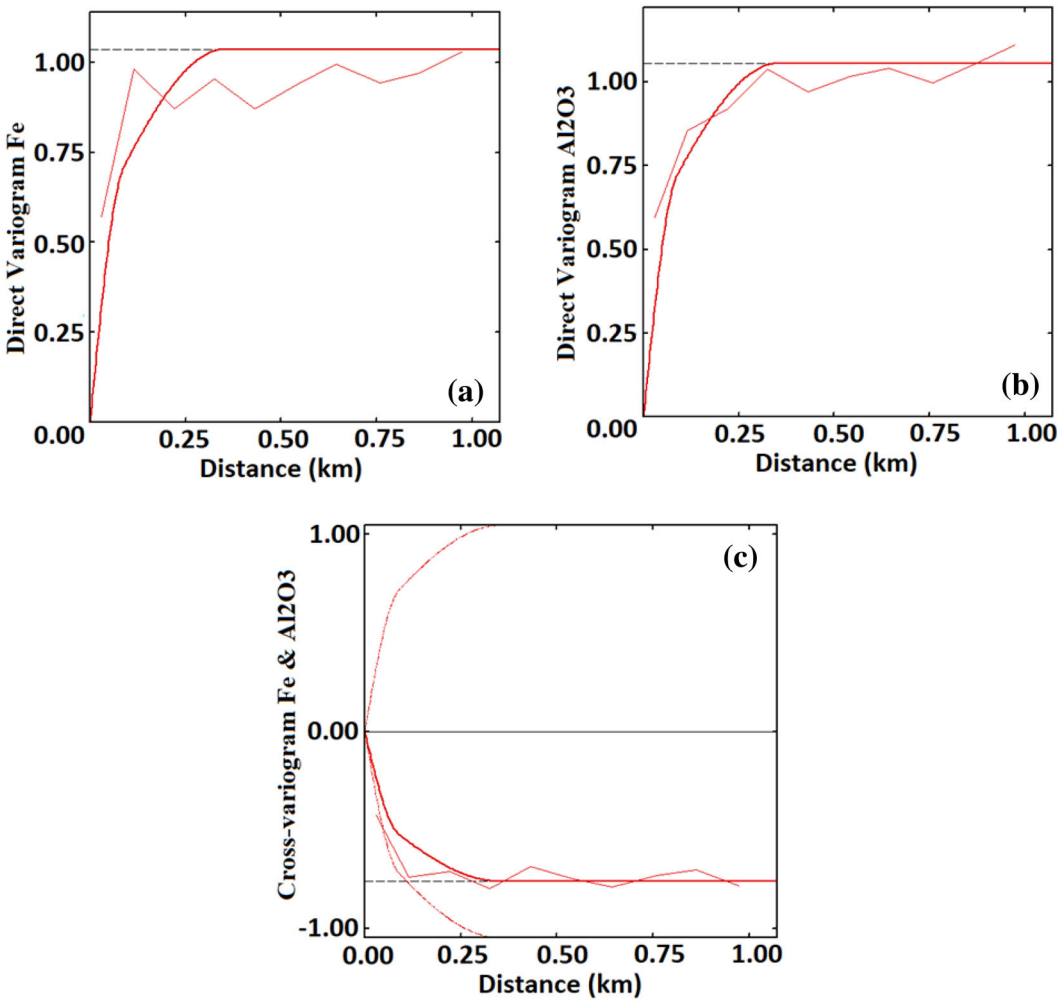

Figure 7. Experimental and theoretical omnidirectional direct (**a**, **b**) and cross-variograms (**c**) of Gaussian Fe and Al_2O_3; negative correlation between the Gaussian random fields shows the negative graph for cross-variogram.

$$\begin{aligned}
&\begin{pmatrix} \gamma_{\mathrm{Fe}}(h) & \gamma_{\mathrm{Fe-Al_2O_3}}(h) \\ \gamma_{\mathrm{Fe-Al_2O_3}}(h) & \gamma_{\mathrm{Al_2O_3}}(h) \end{pmatrix} \\
&= \begin{pmatrix} 0.5185 & -0.3799 \\ -0.3799 & 0.5278 \end{pmatrix} \\
&\quad \mathrm{Spherical}\ (88\ \mathrm{m}, 88\ \mathrm{m}, 88\ \mathrm{m}) \\
&+ \begin{pmatrix} 0.5185 & -0.3799 \\ -0.3799 & 0.5278 \end{pmatrix} \\
&\quad \mathrm{Spherical}(352\ \mathrm{m}, 352\ \mathrm{m}, 352\ \mathrm{m})
\end{aligned} \tag{12}$$

Gaussian Co-simulation Based on the Projection Pursuit Multivariate Transformation (PPMT)

The main privilege of the PPMT is that transformation is built on an iterative algorithm that removes all the complex inter-dependencies, such as heteroscedasticity or nonlinearity, and consequently produces new uncorrelated and normally distributed variables (Adeli et al. 2017). The original declustered data were then converted to PPMT-transformed variables (i.e., PPMT1 and PPMT2) (Fig. 8). The scatterplot between PPMT1 and PPMT2 shows that the two PPMT-transformed variables are perfectly independent.

Following the same steps in the conventional Gaussian co-simulation method, we need to calculate the spatial continuity of the direct and cross-variograms of PPMT1 and PPMT2. However, because of independency characteristics between both PPMT-transformed variables, the conditional co-simulation method can be substituted for the independent simulation over each variable. To do so, the omnidirectional variograms of PPMT1 and PPMT2 were calculated and proper theoretical models were correspondingly fitted, in which two-structured spherical variograms with ranges of 88 m and 352 m were included, respectively (Fig. 9):

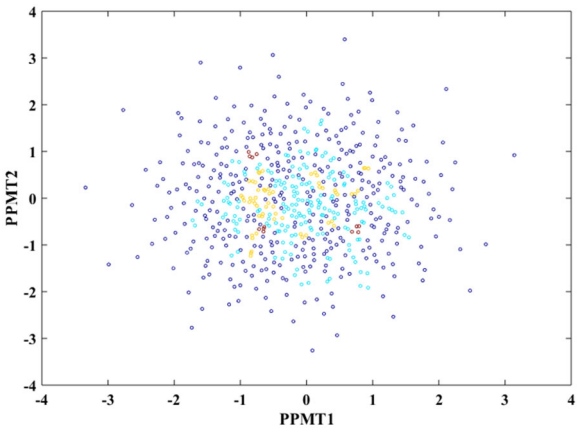

Figure 8. Scatterplot of PPMT-transformed variables; the bivariate distribution of points shows that PPMT1 and PPMT2 are utterly independent.

$$\gamma_{\mathrm{PPMT1}} = 0.5018\ \mathrm{Spherical}(88\ \mathrm{m}, 88\ \mathrm{m}, 88\ \mathrm{m}) + 0.5545\ \mathrm{Spherical}(352\ \mathrm{m}, 352\ \mathrm{m}, 352\ \mathrm{m}) \quad (13)$$

$$\gamma_{\mathrm{PPMT2}} = 0.5018\ \mathrm{Spherical}(88\ \mathrm{m}, 88\ \mathrm{m}, 88\ \mathrm{m}) + 0.5545\ \mathrm{Spherical}(352\ \mathrm{m}, 352\ \mathrm{m}, 352\ \mathrm{m}) \quad (14)$$

The reason for using the omnidirectional variogram is that the PPMT-transformed variables are obtained from the original variables (i.e., Fe and Al_2O_3). Therefore, it is expected that both PPMT1 and PPMT2 show the same spatial continuity structures as the original ones. As already discussed regarding the variography of the original declustered variables, the spatial continuity can be considered omnidirectional because no meaningful special tendencies in the range and sill are identified.

Geostatistical Modeling

Once the variogram analysis was obtained, geostatistical simulation modeling was employed in a grid of 33 m × 42 m × 54 m to model the joint uncertainty of Fe and Al_2O_3 in the region, taking into account their cross-correlation. Three approaches are considered in this section. The first one corresponds to the conventional Gaussian co-simulation via the turning bands co-simulation (Emery 2008) to model the Fe and Al_2O_3 associated with the

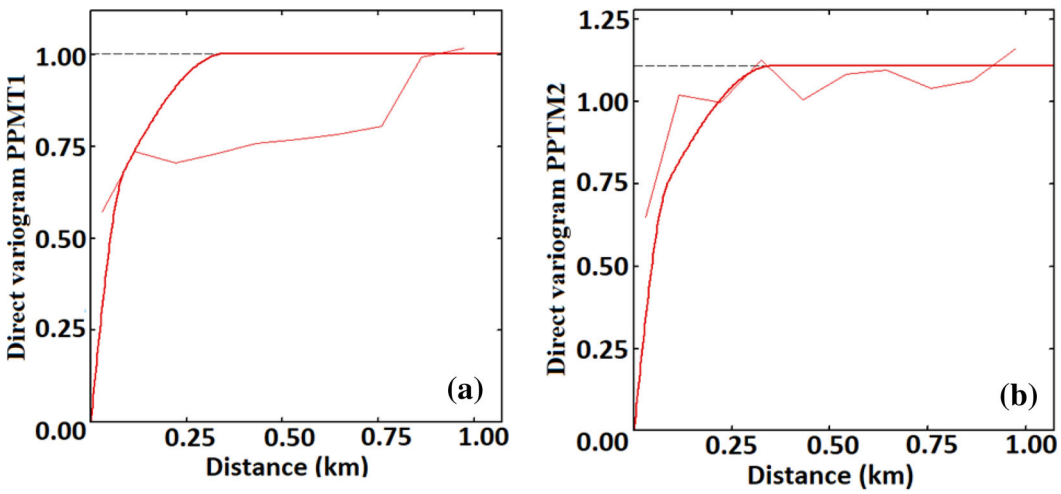

Figure 9. Direct variograms of two underlying decorrelated PPMT-transformed variables by PPMT technique.

linear model of co-regionalizations (hereafter TBCOSIM). The second one is related to the Gaussian co-simulation approach based on the PPMT over the PPMT1 and PPMT2 approaches. Because there is no significant correlation between the PPMT-transformed variables (Fig. 8), an independent simulation can be applied over each PPMT-transformed variable. To do so, a turning bands simulation was separately employed to each PPMT-transformed variable, and then, the results were back-transformed to the original scale (hereafter PPMT). To compare the results, the third family considers independent simulations (turning bands simulation) through the transformed variables obtained from the conventional normal score transformation (hereafter TBSIM). In this case, the direct variograms of the normal score transformed variables were the only functions that were engaged. In all the simulation strategies, a moving neighborhood was selected with parameters set to three times the range of the variograms considering up to a maximum of 80 samples to participate in the estimation. A simple co-kriging method with a multiple search strategy (Madani and Emery 2019) was selected for the turning bands co-simulation, and the simple kriging method in terms of the turning bands simulation was used as a postprocess step for conditioning the non-conditional realizations to the sample locations. To prevent any potential stripping effect, 1000 lines were considered. The number of realizations was deemed to be 100. E-type maps were produced by averaging the 100 realizations of the (co)-simulated elements in each block (Figs. 10, 11).

Validation

The obtained results were considered for the further reproduction of the statistical analysis validation. It was of interest to examine different approaches applied in this research to validate the outputs. This step was important because it directly impacts the trustworthiness of the underlying co-simulation methodology for mineral resource classification.

Spatial Statistical Analysis

The first test examines the reproducibility of the spatial cross-correlation among Fe and Al_2O_3 in the region. The cross-correlograms are presented for the original declustered Fe, namely the simulation obtained from the TBSIM, TBCOSIM and PPMT in Figure 12. The results show that the cross-correlograms of the TBCOSIM and PPMT are fairly similar to original declustered Fe and behave similar to the cross-correlogram of the original declustered Fe. Therefore, the TBCOSIM and PPMT can reproduce the spatial correlation because these two methodologies take into account the inter-dependency between the covariables: the former through the linear model of co-regionalization and the latter through the factorization steps. However, as expected, the TBSIM was not able to reproduce the shape of the cross-correlogram because it simulates each variable independently.

Global Statistical Analysis

The declustered mean of Fe and Al_2O_3 was compared with the average mean of the simulated and back-transformed variables through 100 realizations obtained from the TBCOSIM, TBSIM and PPMT. As shown in Figure 13, the average mean of Fe and Al_2O_3 is less than the declustered mean of the original variables in both the TBCOSIM and TBSIM outputs. However, in the PPMT, the average line over the realizations corroborates that the realizations are dramatically able to reproduce the original declustered mean value for both Fe and Al_2O_3.

Another comparison was made on the variance of the declustered values with an average variance value over 100 simulated realizations of the aforementioned three methodologies. The average variances of the TBSIM and TBCOSIM are higher for Fe and less for Al_2O_3 compared to the declustered variance for both variables (Fig. 14). However, in the PPMT, the average variance mimics the original declustered variance for both Fe and Al_2O_3.

The last examination considers the global correlation coefficients between Fe and Al_2O_3 obtained from the three approaches by comparing with the original declustered correlation coefficient. Figure 15 shows the difference between the original correlation coefficient and the reproduced average correlation coefficient over 100 realizations. The worst reproduction with almost zero correlation manifests itself in the TBSIM results. This approximately zero correlation coefficient can be explained by the fact that independent simulation does not consider the intrinsic correlation between covari-

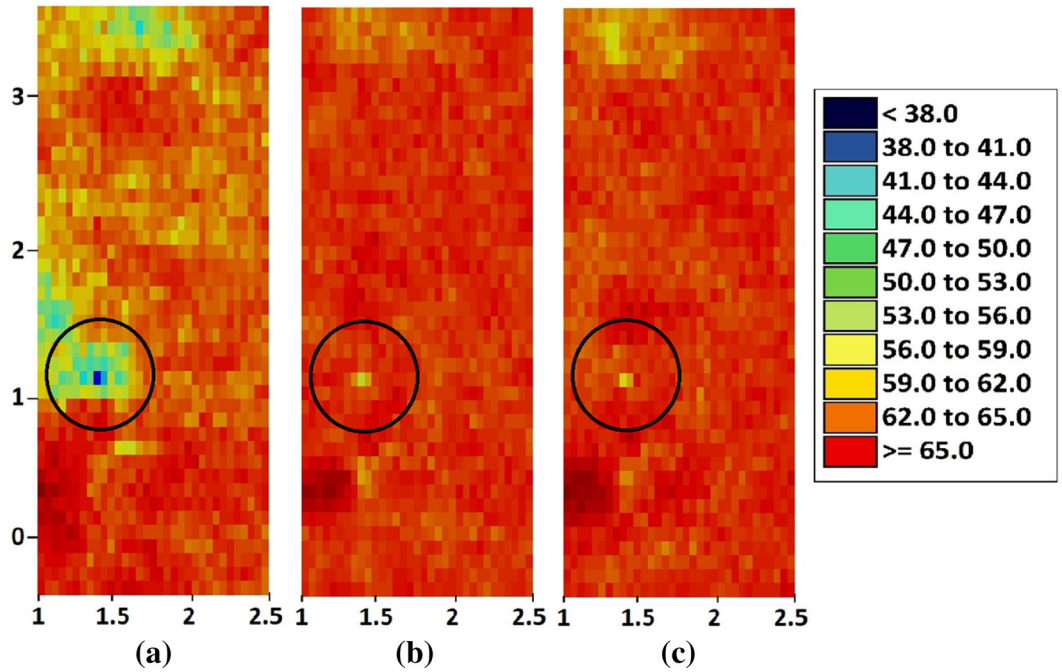

Figure 10. E-type models of Fe for (**a**) PPMT, (**b**) TBCOSIM and (**c**) TBSIM obtained from 100 realizations. The most significant differences among three approaches can be recognized in the black circles.

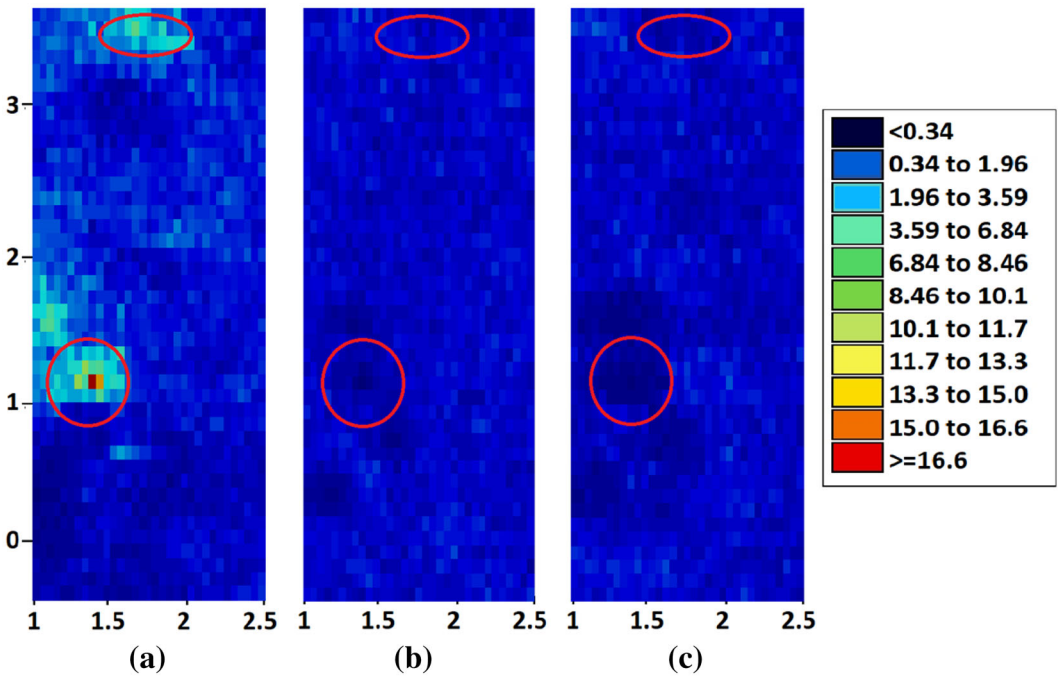

Figure 11. E-type models of Al_2O_3 for PPMT (left), TBCOSIM (middle) and TBSIM (right) obtained from 100 realizations. The most significant differences among three approaches can be recognized through the red circles.

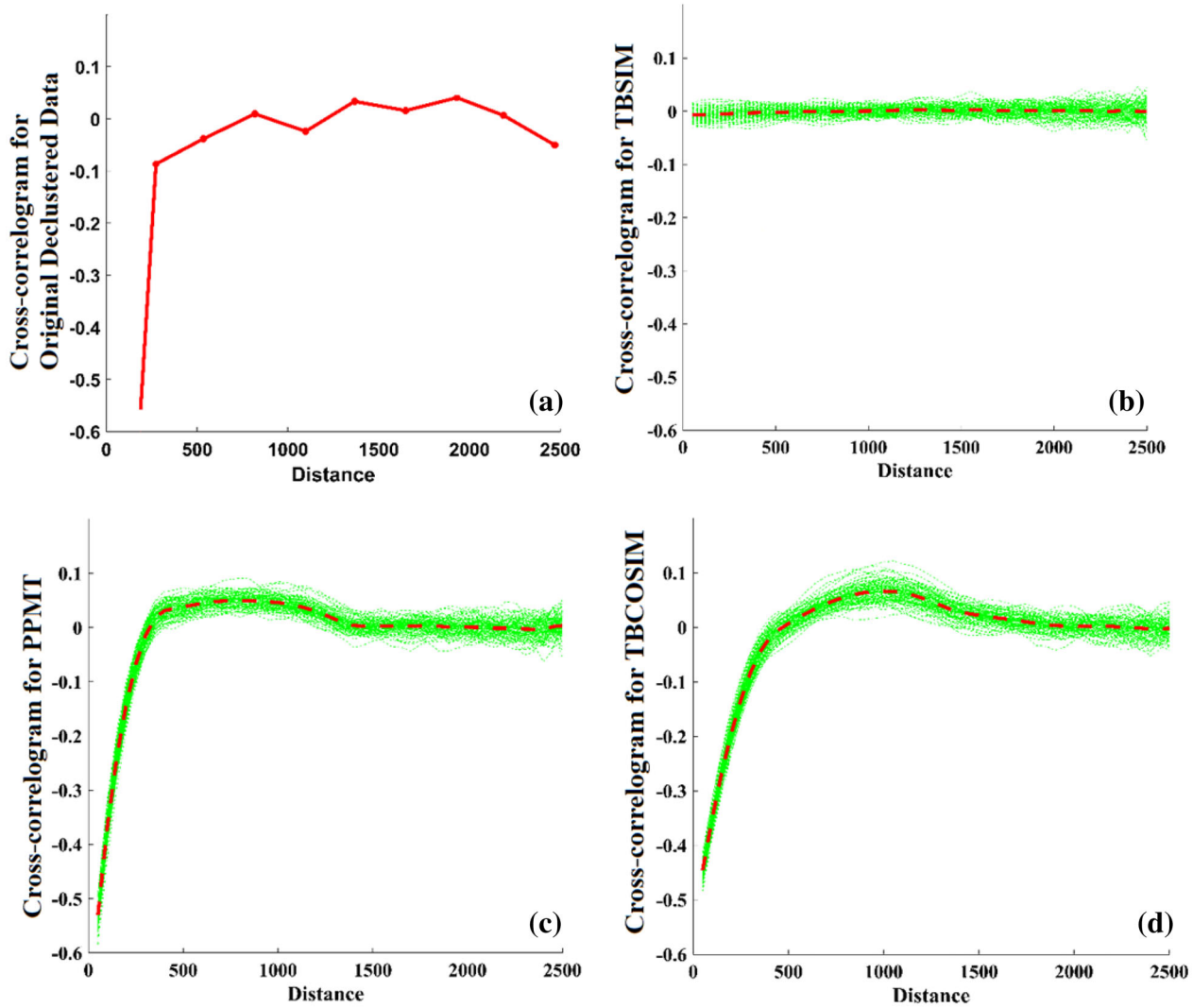

Figure 12. Cross-correlogram for (**a**) original declustered data, (**b**) TBSIM, (**c**) TBCOSIM and (**d**) PPMT. Average (red line) and 100 individual realizations (green lines).

ables in the multi-element deposits (Madani and Ortiz 2017; Maleki and Madani 2017; Eze et al. 2019; Abildin et al. 2019). The TBCOSIM methodology presents a better result with an average correlation coefficient of almost 0.57, although it is not considered as a reliable result. The affecting condition for this type of poor reproduction of the correlation coefficient may be because of the complex inter-dependency between covariables (Fe and Al_2O_3), leading to such an inadequate measure of correlation. However, the results from the PPMT show that this approach can effectively handle the complex inter-dependencies between covariables and is capable of reproducing the original declustered correlation coefficient on average.

MINERAL RESOURCE CLASSIFICATION

Mineral resource classification is vital in the uncertainty assessment and risk analysis for mineral resource development. One of the sub-processing steps of realizations is mineral resource classification based on international standards such as the JORC code. The JORC code is the Australian Code for reporting the results of exploration, mineral re-

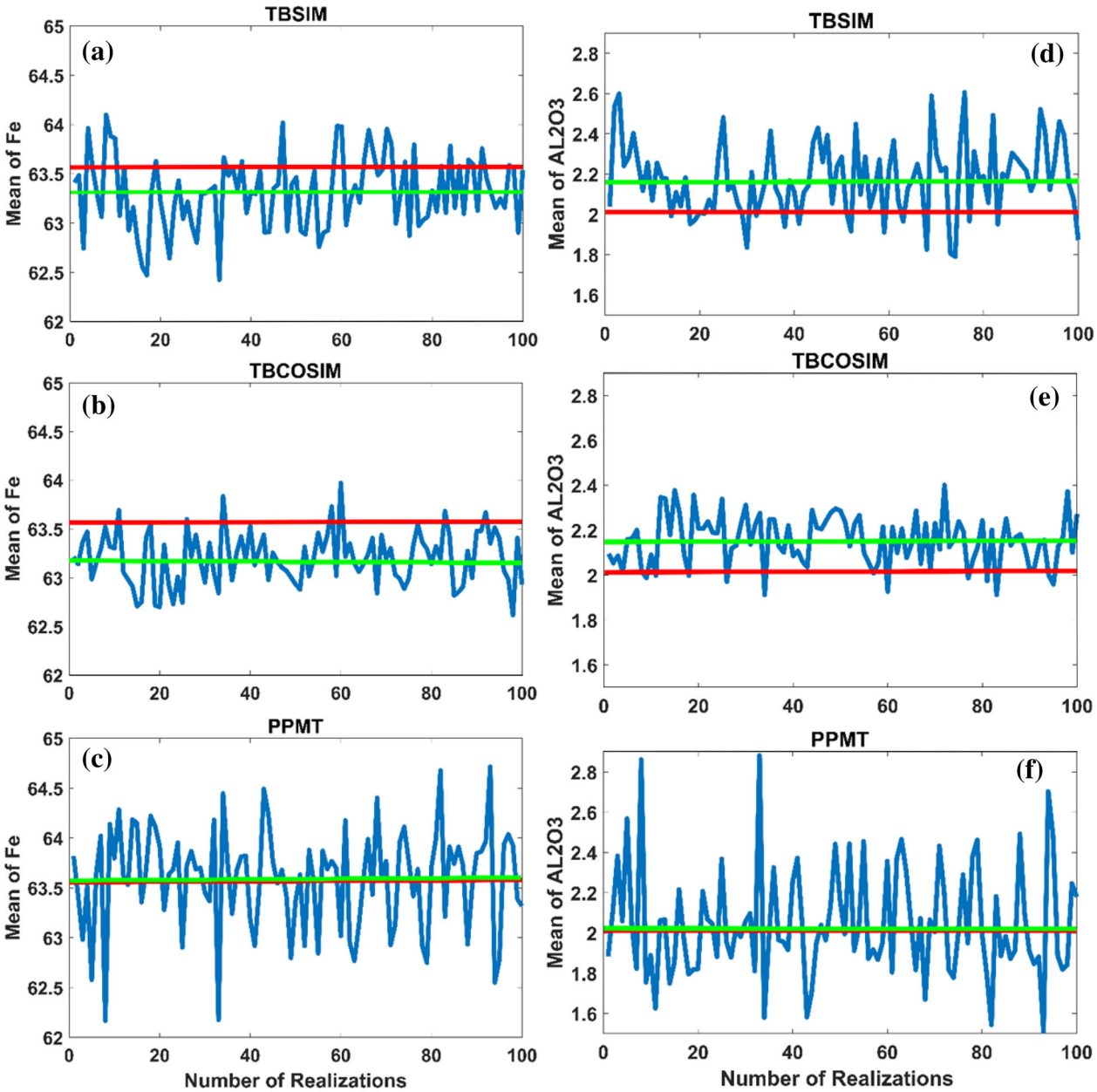

Figure 13. Mean of iron (Fe) (**a**–**c**) and aluminum oxide (Al_2O_3) (**d**–**f**) from TBSIM (**a**, **d**), TBCOSIM (**b**, **e**) and PPMT (**c**, **f**) methodologies. Red line indicates declustered means of Fe and Al_2O_3; green line indicates the average mean of 100 realizations; blue line is the corresponding statistical parameter for each realization.

sources and ore reserves. The reporting of mineral resources is based on the economic interest in the Earth's crust for the extraction of solid materials with eventual profitability. Mineral resources are subdivided into inferred, indicated and measured categories based the level of confidence depending on the knowledge and geologic evidence comprising the sampling results. This classification is necessary for mine planning steps, for which some parts of either the measured or indicated categories can be converted to minable sections. Thereafter, modifying factors, such as mining, processing, metallurgical, infrastructure, economic, marketing, legal, environment, social and government can be employed, particularly regarding the final decision of a competent person (JORC 2012).

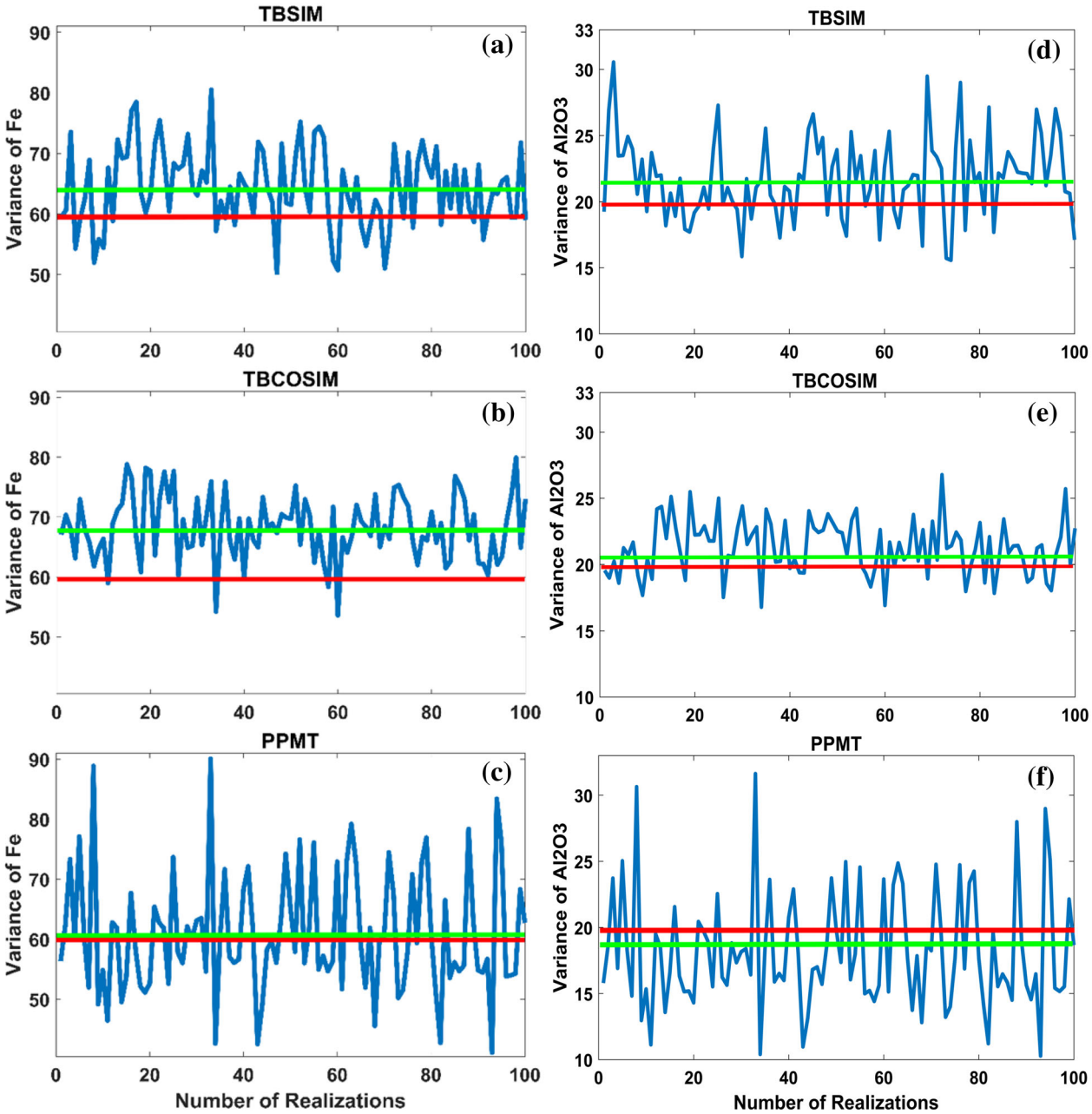

Figure 14. Variance of iron (Fe) (**a**–**c**) and aluminum oxide (Al_2O_3) (**d**–**f**) from TBSIM (**a**, **d**), TBCOSIM (**b**, **e**) and PPMT (**c**, **f**) methodologies. Red line indicates declustered variance of Fe and Al_2O_3; green line indicates the average variance of 100 realizations; blue line is the corresponding statistical parameter for each realization.

The main idea of this research was to compare the three different approaches of simulations based on two main Gaussian transformation techniques (one based on the conventional Gaussian transformation and one based on the PPMT). Compared to the TBSIM and TBCOSIM approaches, the PPMT results corroborate that not only the realizations can reproduce global statistics but they can also reliably reproduce local statistics, which is an important supposition in the further analysis of a mining project. For instance, as shown in Figure 10, the E-type map, which is the average of 100 realizations of the PPMT, shows less Fe content at the center (black circles areas) and top of the map, while the E-type

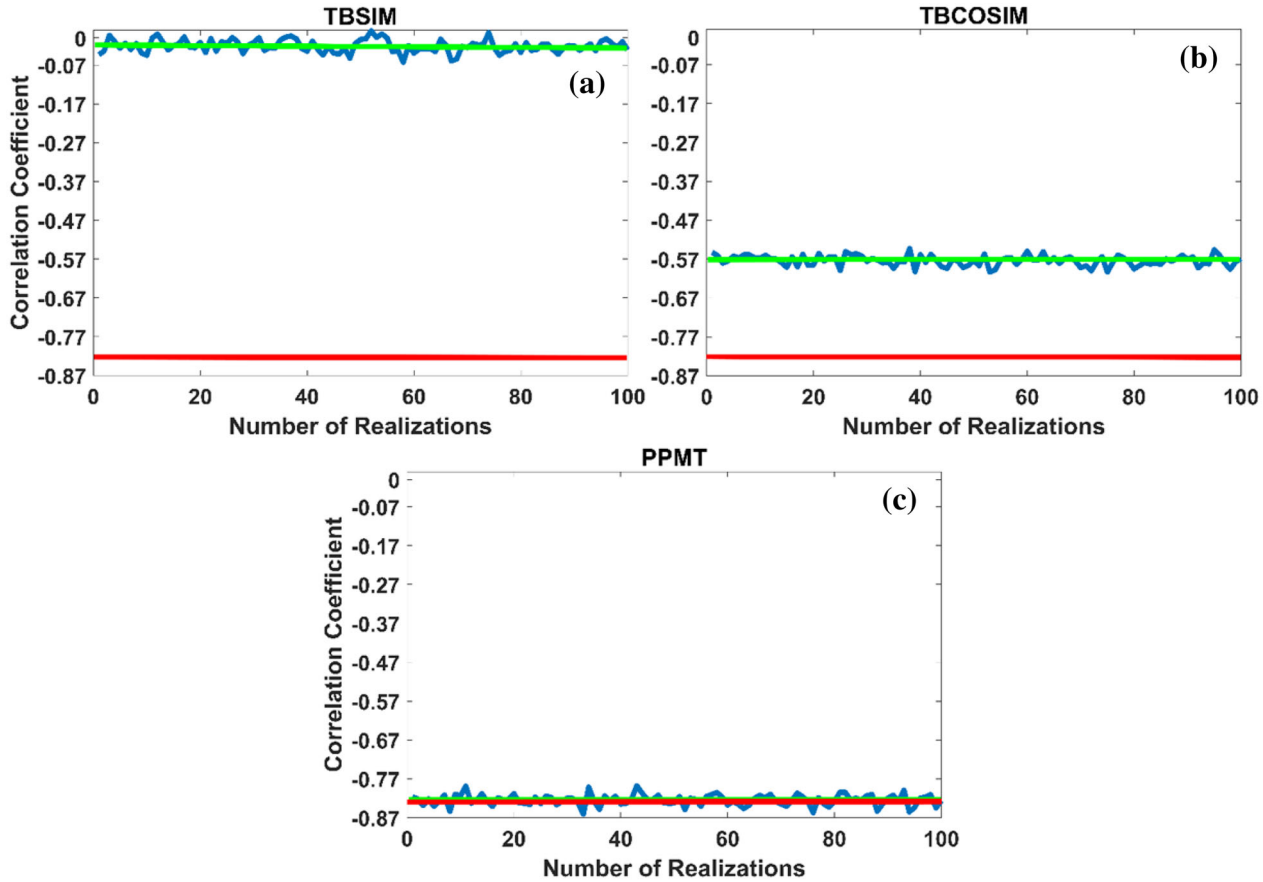

Figure 15. Correlation coefficients between iron (Fe) and aluminum oxide (Al_2O_3) of 100 realizations from (**a**) TBSIM, (**b**) TBCOSIM and (**c**) PPMT methodologies. Red line indicates original correlation coefficient between of Fe and Al_2O_3; green line indicates the average correlation coefficient of 100 realizations; blue line is the corresponding correlation coefficient for each realization.

maps from the TBSIM and TBCOSIM methods indicate a higher concentration of Fe with a small difference on the same level. This dispute is also examined between the E-type maps of the PPMT and the two other methodologies. The results indicate that the same analogous feature can be observed on the E-type maps of Al_2O_3 (Fig. 11), where the TBCOSIM and TBSIM show fairly low concentrations (red circled areas), whereas the PPMT map illustrates a high content of Al_2O_3. As the intrinsic correlation was perfectly reproduced in the PPMT, the E-type maps of this method directly support the negative correlation between Fe and Al_2O_3 during visual inspection. In contrast, the TBCOSIM and TBSIM approaches do not support this feature, which means that these methodologies cannot handle the complexity in multi-element deposits.

Because the results of the PPMT method are more reasonable and satisfactory in practice, the use of this method is encouraged for the classification of the mineral resources in the underlying Fe deposit into measured, indicated and inferred resources based on the JORC code. However, to show the difference between the methodologies, the tonnages are calculated within the realizations obtained from three methods (PPMT, TBSIM and TBCOSIM), depending on the cutoff grades of Fe (35%, 40%, 45%, 50%, 55%, 60% and 65%) (Table 2). The resource classification based on uncertainty models is quantified as measured if the block is known within ± 15% (90% of the time); as an indicated resource if the block is known within ± 15% and ± 30% (90% of the time) and as an inferred resource if the block is known more than ± 30% (Rossi and Deutsch 2014). The outputs for the resource classifications are then compared and discussed.

In almost all cases, the total tonnage of the PPMT is higher than that of either the TBCOSIM or

Table 2. Mineral resource classification and calculation of tonnage in each category for Fe in Carajas ore deposit through the simulation results obtained from PPMT, TBSIM and TBCOSIM approaches

Methods	Cutoff grade	Measured (Mt)	Indicated (Mt)	Inferred (Mt)	Total tonnage (Mt)
TBSIM	35	11,360.00	971.94	1274.10	13,606.04
	40	11,349.00	963.97	1096.30	13,409.27
	45	11,337.00	939.20	913.82	13,190.02
	50	11,320.00	759.66	854.74	12,934.40
	55	11,266.00	585.35	842.36	12,693.71
	60	10,756.00	416.38	799.77	11,972.15
	65	8239.40	354.43	608.34	9202.17
TCOSIM	35	11,081.00	1016.40	1469.80	13,567.20
	40	11,068.00	1007.30	1287.30	13,362.60
	45	11,054.00	979.50	1104.50	13,138.00
	50	11035.00	799.68	1043.80	12,878.48
	55	10,978.00	628.85	1028.30	12,635.15
	60	10,472.00	464.92	975.92	11,912.84
	65	8042.00	399.36	747.40	9188.76
PPMT	35	11,643.00	747.40	1178.10	13,568.50
	40	11,635.00	740.70	1042.10	13,417.80
	45	11,629.00	724.23	941.72	13,294.95
	50	11,614.00	537.73	896.55	13,048.28
	55	11,586.00	435.89	888.92	12,910.81
	60	11,046.00	328.34	845.81	12,220.15
	65	8519.90	274.05	648.64	9442.59

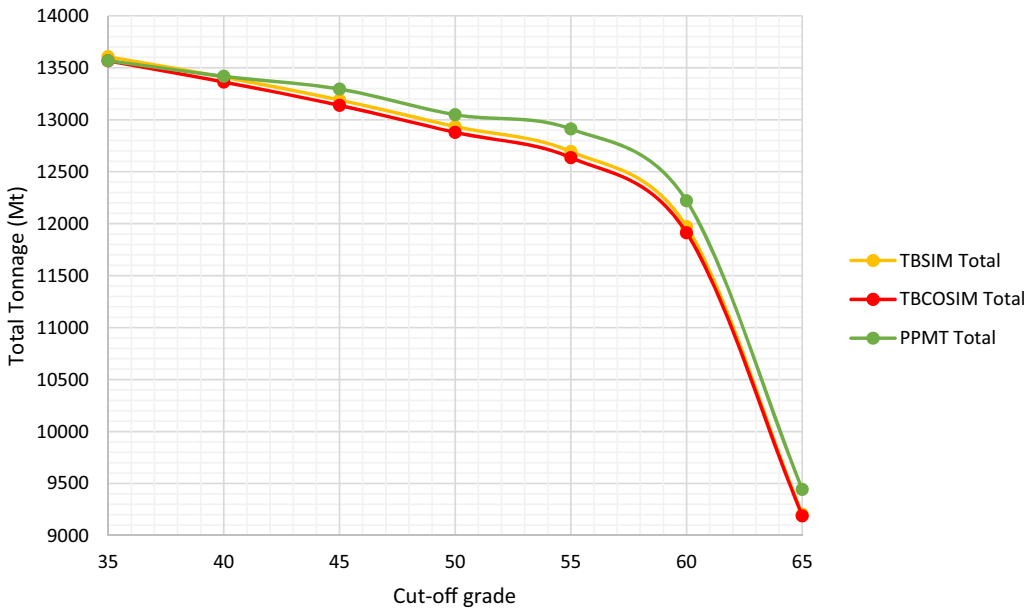

Figure 16. Total tonnage vs. cutoff grade.

the TBSIM (Fig. 16). In real life, these types of crucial differences in the results of the total tonnage play a vital role with regard to financial issues for mining companies. The comparison of the measured mineral resources of each method is quite significant due to the level of confidence in this category, which

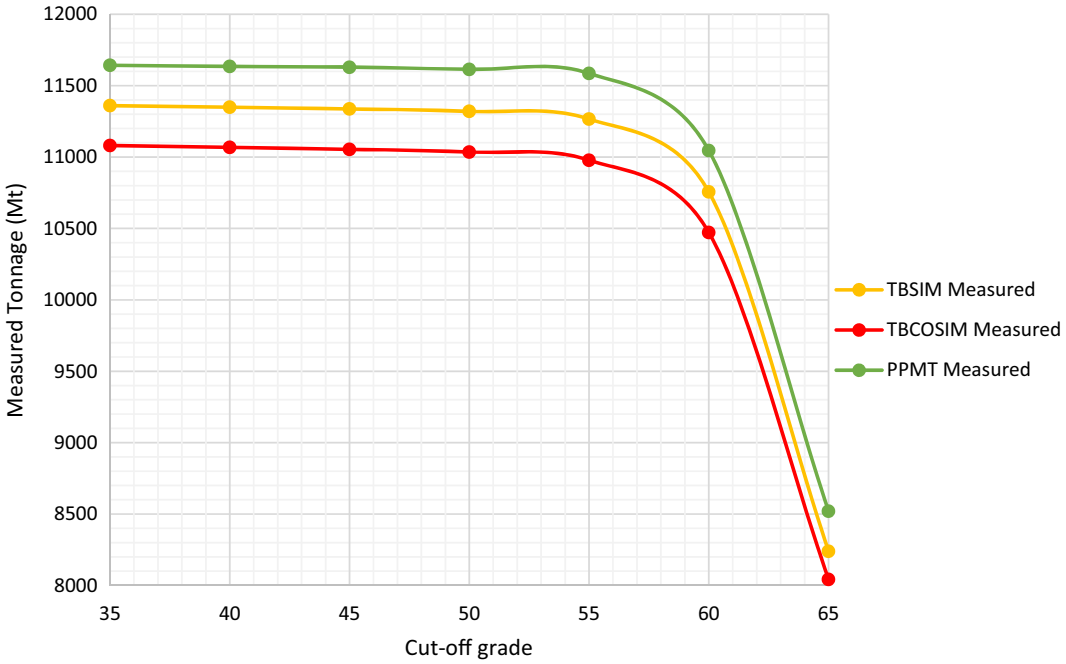

Figure 17. Measured tonnage vs. cutoff grade.

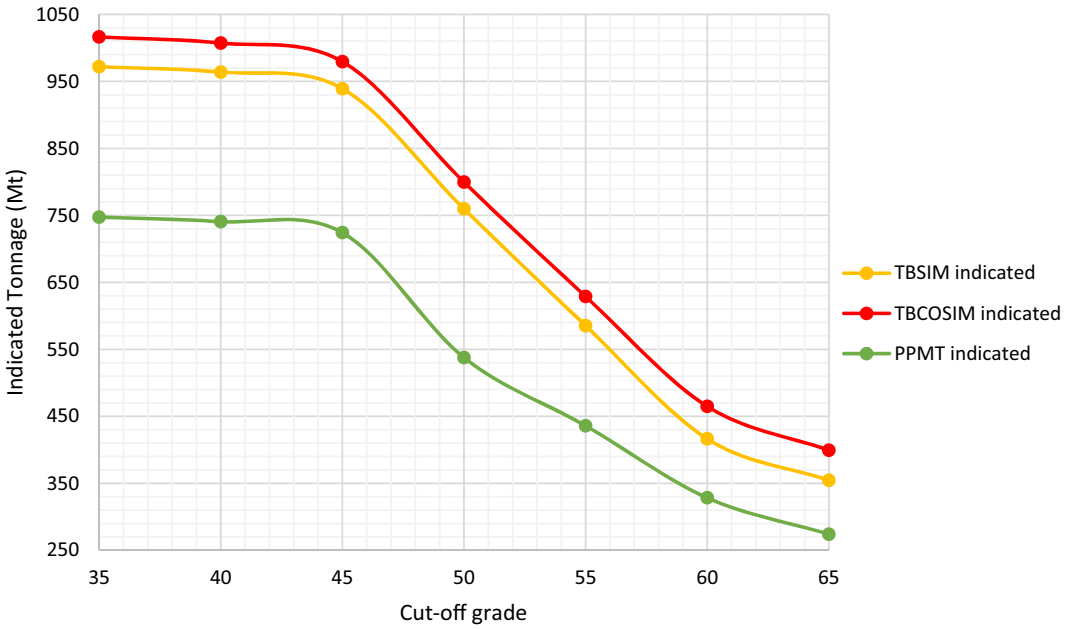

Figure 18. Indicated tonnage vs. cutoff grade.

leads to the critical further analysis and planning of a mining project. The PPMT methodology provides the highest tonnage within all cutoff grades (Fig. 17). For the indicated resources (Fig. 18), the PPMT provides small tonnages for all the cutoff grades, and in the inferred category (Fig. 19), only

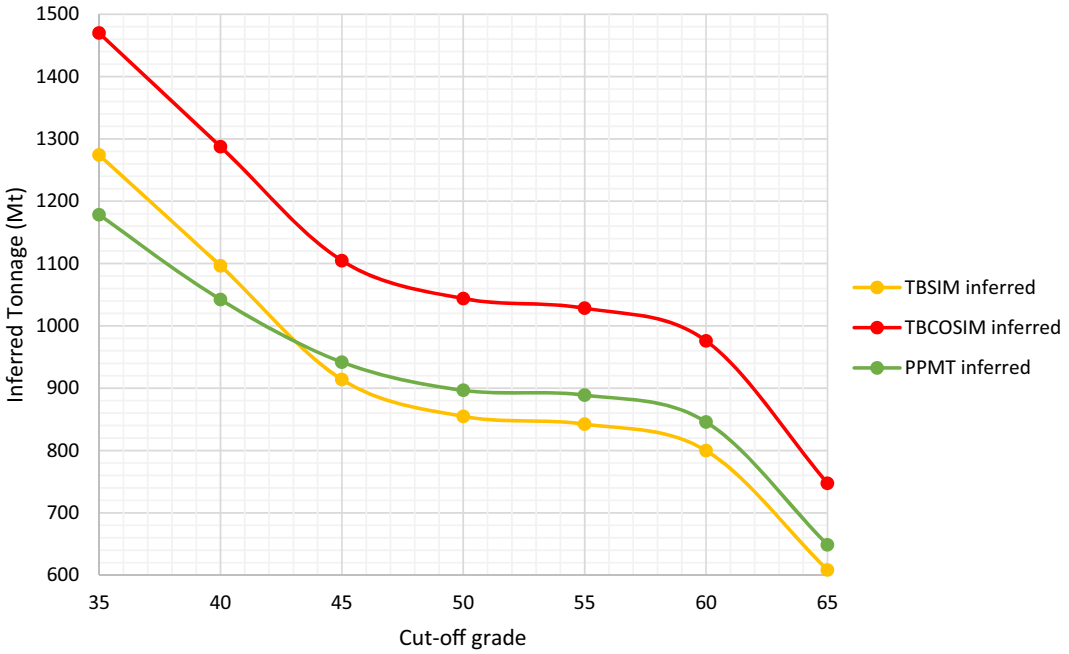

Figure 19. Inferred tonnage vs. cutoff grade.

the TBCOSIM provides the highest values of tonnages for each cutoff grade. Notably, the tonnage in the indicated and inferred categories is not as high as that obtained from the TBCOSIM and TBSIM. This significant difference should be seriously considered whenever the conventional Gaussian co-simulation or independent simulation are employed in mineral resource classification.

The application of these methods not only affects the resource estimation but also affects the cash flow of the project, the net present value (NPV) calculation, the geometry of the optimal open pit and the identification of useful blocks. Due to the different results mentioned above for each method and the confirmation of the reliability in the PPMT simulation results, the PPMT technique is recommended for deposits with complex inter-dependencies between covariables over conventional Gaussian independent simulations and co-simulations, which show inadequate performance for the reproduction of the spatial and global correlations and thus the resource estimation and its classification.

CONCLUSIONS

Geostatistical simulation methods are becoming more popular than estimation methods due to their reliability on the spatial grade distribution and their ability to provide multiple scenarios, while estimation methods result in unique scenarios. However, the increasing demand for properly executed simulation methods for resource estimations to obtain more reliable block models for mine projects has led to the investigation and modernization of simulation techniques. In this paper, three simulation methods were compared and employed in the mineral resource classification of an Fe deposit wherever there is a good correlation between Fe and Al_2O_3. As mentioned earlier, it is difficult for the independent simulation method to reproduce the correlation coefficient because of its inability to take into account the intrinsic correlation between covariables. Although the co-simulation method is based on conventional Gaussian transformation that considers the intrinsic correlation between covariables, it showed unreliable results in the reproduction of the local and global cross-correlation coefficients. In contrast, the PPMT methodology showed a positive performance regarding the reproduction of the correlation coefficient. The results in mineral resource estimation via the above-mentioned three methods also provided different outputs with respect to tonnage evaluation. Furthermore, the idea of this paper was to show that employing a proper geostatistical simulation algorithm impacts definitely the further analysis of a mining project such as mineral resource

categorization, following an international standard such as the JORC code. Through the paper, it was shown mathematically that the PPMT approach outperforms the independent and joint simulation in terms of reproducing the statistical parameters, leading to different tonnages for all different categories (i.e., measured, indicated and inferred). One of the aim of this paper concerning this issue is that employing a proper geostatistical simulation algorithm does not necessarily imply that output of tonnage calculation should be as high as possible. Conversely, even utilizing a suitable algorithm may provide much less tonnage compared to other methods that deliver biasedly pseudo high tonnage. The application of the PPMT methodology is highly encouraged for multi-element deposits wherever there exists a complex inter-dependency among covariables. This method accounts for better global and spatial statistical parameters and correlation reproduction, leading to a better estimation and classification of mineral resources based upon international standards.

ACKNOWLEDGMENTS

The authors are grateful to Nazarbayev University for funding this work via ''Faculty Development Competitive Research Grants for 2018–2020 under Contract No. 090118FD5336.'' The second author acknowledges the Social Policy Grant (SPG) supported by Nazarbayev University. The authors also thank the Geovariances Company for providing the dataset. We are also grateful to Dr. John Carranza and the reviewers for their valuable comments, which substantially helped improving the final version of the manuscript.

REFERENCES

Abildin, Y., Madani, N., & Topal, E. (2019). A hybrid approach for joint simulation of geometallurgical variables with inequality constraint. *Minerals, 9*(1), 24.

Adeli, A., Emery, X., & Dowd, P. (2017). Geological modelling and validation of geological interpretations via simulation and classification of quantitative covariates. *Minerals, 8*(1), 7.

Arik, A. (1999). An alternative approach to ore reserve classification. In *APCOM proceedings of the 1999 computer applications in the mineral industries (APCOM) symposium* (pp. 45–53).

Arik, A. (2002). Comparison of resource classification methodologies with a new approach. In *APCOM proceedings of the 2002 application of computers and operations research in the mineral industry (APCOM) symposium* (pp 57–64).

Barnett, R., Manchuk, J., & Deutsch, C. (2014). Projection pursuit multivariate transform. *Mathematical Geosciences, 46*(3), 337–359.

Barnett, R. M. (2017). Projection pursuit multivariate transform. In J. L. Deutsch (Ed.), *Geostatistics lessons*. http://www.geostatisticslessons.com/lessons/lineardecorrelation.html. Accessed 24 Oct 2018.

Barnett, R. M., Manchuk, J. G., & Deutsch, C. V. (2016). The projection pursuit multivariate transform for improved continuous variable modeling. *Society of Petroleum Engineers*. https://doi.org/10.2118/184388-pa.

Beisiegel, V. D. R., Bernardelli, A. L., Drummond, N. F., Ruff, A. W., & Tremaine, J. W. (1973). Geologia e recursos minerais da Serra dos Carajás. *Brazilian Journal of Geology, 3*(4), 215–242.

Boisvert, J. B., Rossi, M. E., Ehrig, K., & Deutsch, C. V. (2013). Geometallurgical modeling at Olympic dam mine, South Australia. *Mathematical Geosciences, 45*(8), 1–25.

Carr, J. R., & Myers, D. E. (1985). COSIM: A FORTRAN IV program for coconditional simulation. *Computers & Geosciences, 11*(6), 675–705.

Chilès, J. P., & Delfiner, P. (2012). *Geostatistics: Modeling spatial uncertainty* (2nd ed.). New York: Wiley.

Code, J. O. R. C., & Joint Ore Reserves Committee. (2012). The JORC code and guidelines. Australasian code for reporting of exploration results, mineral resources and ore reserves prepared by The Australasian Institute of Mining and Metallurgy (AusIMM), Australian Institute of Geoscientists and Minerals Council of Australia. [Online] Dostępne w: www.jorc.org [Dostęp: 10.07. 2015].

David, M. (1977). *Geostatistical ore reserve estimation*. New York: Elsevier Science Publishing Co.

Deutsch, C. (1989). DECLUS: A FORTRAN 77 program for determining optimum spatial declustering weights. *Computers & Geosciences, 15*(3), 325–332.

Deutsch, C. V. (2013). Geostatistical modelling of geometallurgical variables: Problems and solutions. In S. Dominay (Eds.), *Proceeding of the second AusIMM international geometallurgy conference (Geomet 2013)*. Brisbane, Australia.

Deutsch, C. V., & Journel, A. G. (1998). *Geostatistical software library and user's guide*. New York: Oxford University Press.

Deutsch, C. V., Leuangthong, O., & Ortiz J. (2006). A case for geometric criteria in resources and reserves classification. Centre for Computational Geostatistics, report 7, University of Alberta, Edmonton.

Dimitrakopoulos, R., Godoy, M., & Chou, C. (2009). Resource/reserve classification with integrated geometric and local grade variability measures. In *Proceedings orebody modelling and strategic mine planning* (pp. 207–214). The Australasian Institute of Mining and Metallurgy, Melbourne.

Dohm, C. (2005). Quantifiable mineral resource classification: A logical approach. In O. Leuanthong & C. V. Deutsch (Eds.), *Geostatistics Banff 2004* (Vol. 1, pp. 333–342). Dordrecht: Kluwer Academic Publishers.

Dominy, S. C., Noppé, M. A., & Annels, A. E. (2002). Errors and uncertainty in mineral resource and ore reserve estimation: The importance of getting it right. *Exploration and Mining Geology, 11*(1–4), 77–98.

Duggan, S., & Dimitrakopoulos, R. (2005). Application of conditional simulation to quantify uncertainty and to classify a diamond deflation deposit. In O. Leuangthong & C. Deutsch (Eds.), *Geostatistics Banff 2004* (Vol. 2, pp. 419–428). Dordrecht: Kluwer Academic Publishers.

Emery, X. (2005). Simple and ordinary multigaussian kriging for estimating recoverable reserves. *Mathematical Geology, 37*(3), 295–319.

Emery, X. (2007). Conditioning simulations of Gaussian random fields by ordinary kriging. *Mathematical Geology, 39*(6), 607–623.

Emery, X. (2008). A turning bands program for conditional co-simulation of cross-correlated Gaussian random fields. *Computers & Geosciences, 34*(12), 1850–1862.

Emery, X., & Lantuéjoul, C. (2006). Tbsim: A computer program for conditional simulation of three-dimensional gaussian random fields via the turning bands method. *Computers & Geosciences, 32*(10), 1615–1628.

Emery, X., Ortiz, J. M., & Rodríguez, J. J. (2006). Quantifying uncertainty in mineral resources by use of classification schemes and conditional simulations. *Mathematical Geology, 38*(4), 445–464.

Eze, P. N., Madani, N., & Adoko, A. C. (2019). Multivariate mapping of heavy metals spatial contamination in a Cu–Ni exploration field (Botswana) using turning bands co-simulation algorithm. *Natural Resources Researches, 28*(1), 109–124. https://doi.org/10.1007/s11053-018-9378-3.

Fox, K. A. (2017). The usefulness of NI 43-101 technical reports for financial analysts. *Research Policy, 51,* 225–233.

Friedman, J. H. (1987). Exploratory projection pursuit. *Journal of American Statistical Association, 82,* 249–266.

Goovaerts, P. (1997). *Geostatistics for natural resources evaluation*. New York: Oxford University Press.

Gutjahr, A., Bullard, B., & Hatch, S. (1997). General joint conditional simulations using a fast Fourier transform method. *Mathematical Geology, 29*(3), 361–389.

Holdsworth, R. E., & Pinheiro, R. V. (2000). The anatomy of shallow-crustal transpressional structures: Insights from the Archaean Carajás fault zone, Amazon, Brazil. *Journal of Structural Geology, 22*(8), 1105–1123.

Hosseini, S. A., & Asghari, O. (2018). Multivariate geostatistical simulation on block-support in the presence of complex multivariate relationships: Iron ore deposit case study. *Natural Resources Researches*. https://doi.org/10.1007/s11053-018-9379-2.

Journel, A. G., & Huijbregts, C. J. (1978). *Mining geostatistics*. London: Academic Press.

Krige, D. G. (1996). A practical analysis of the effects of spatial structure and of data available and accessed, on conditional biases in ordinary kriging. *Geostatistics Wollongong, 96,* 799–810.

Krige, D. G. (1999). Conditional bias and uncertainty of estimation in geostatistics. In *Keynote address for APCOM, 99*.

Krzemień, A., Fernández, P. R., Sánchez, A. S., & Álvarez, I. D. (2016). Beyond the pan-european standard for reporting of exploration results, mineral resources and reserves. *Resources Policy, 49,* 81–91.

Lantuéjoul, C. (1994). Non conditional simulation of stationary isotropic multigaussian random functions. In M. Armstrong & P. A. Dowd (Eds.), *Geostatistical simulations* (pp. 147–177). Dordrecht: Springer.

Lantuéjoul, C. (2002). *Geostatistical simulation, models and algorithms* (p. 256). Berlin: Springer.

Leuangthong, O., & Deutsch, C. V. (2003). Stepwise conditional transformation for simulation of multiple variables. *Mathematical Geology, 35*(2), 155–173.

Madani, N., & Emery, X. (2019). A comparison of search strategies to design the cokriging neighborhood for predicting coregionalized variables. *Stochastic Environmental Research and Risk Assessment*, *33*(1), 183–199. https://doi.org/10.1007/s00477-018-1578-1.

Madani, N., & Ortiz, J. (2017). Geostatistical simulation of cross-correlated variables: A case study through Cerro Matoso Nickel-Laterite deposit. In *The 26th international symposium on mine planning and equipment selection*. Nazarbayev University School of Mining and Geosciences.

Maleki, M., & Madani, N. (2017). Multivariate geostatistical analysis: An application to ore body evaluation. *Iranian Journal of Earth Sciences, 8,* 173–184.

Manchuk, J., Leuangthong, O., & Deutsch, C. (2009). The proportional effect. *Mathematical Geosciences, 41*(7), 799–816.

Matheron, G. (1973). The intrinsic random functions and their applications. *Advances in Applied Probability, 5*(3), 439–468.

Meirelles, E. M., Hirata, W. K., Amaral, A. D., Medeiros Filho, C. A., & Gato, W. D. C. (1984). Geologia das folhas Carajás e Rio Verde, Província Mineral de Carajás, Estado do Pará. In Congresso Brasileiro de Geologia, no. 33, Rio de Janeiro, Annals (Vol. 5, pp. 2164–2174).

Menin, R., Diedrich, C., Reuwsaat, J. D., & De Paula, W. F. (2017). Drilling grid analysis for defining open-pit and underground mineral resource classification through production data. In J. Gómez-Hernández, J. Rodrigo-Ilarri, M. Rodrigo-Clavero, E. Cassiraga, & J. Vargas-Guzmán (Eds.), *Geostatistics valencia (2016). Quantitative geology and geostatistics* (Vol. 19). Cham: Springer.

Murphy, M., Parker, H., Ross, A., & Audet, M. (2004). Ore-thickness and nickel grade resource confidence at the Koniambo nickel laterite deposit in New Caledonia: A conditional simulation voyage of discovery. In O. Leuangthong & C. Deutsch (Eds.), *Geostatistics Banff 2004*. Dordrecht: Springer.

Mwasinga, P. (2001). Approaching resource classification: General practices and the integration of geostatistics. In *Proceedings of the 2001 international symposium on computer applications in the mineral industries (APCOM)* (pp. 97–104).

Myers, D. E. (1989). Vector conditional simulation. In M. Armstrong (Ed.), *Geostatistics* (pp. 283–293). Dordrecht: Kluwer Academic.

Naus, T. (2008). Unbiased LiDAR data measurement (draft). Retrieved September 20, 2018 from http://www.asprs.org/a/society/committees/lidar/Unbiased_measurement.pdf.

Paradella, W. R., Ferretti, A., Mura, J. C., Colombo, D., Gama, F. F., Tamburini, A., et al. (2015). Mapping surface deformation in open pit iron mines of Carajás Province (Amazon Region) using an integrated SAR analysis. *Engineering Geology, 193,* 61–78.

Paravarzar, S., Emery, X., & Madani, N. (2015). Comparing sequential Gaussian simulation and turning bands algorithms for cosimulating grades in multi-element deposits. *Comptes Rendus Geoscience, 347*(2), 84–93.

Reed, M., & Simon, B. (1972). Methods of modern mathematical physics: Functional analysis. *Resources Policy, 49*(2016), 81–91.

Rivoirard, J. (1994). *Introduction to disjunctive kriging and non-linear geostatistics*. Oxford: Clarendon Press.

Rivoirard, J., & Renard, D. (2016). A specific volume to measure the spatial sampling of deposits. *Mathematical Geosciences, 48*(7), 791–809.

Rossi, M. E. (2003). Practical aspects of large-scale conditional simulations. In *Proceedings of the 31st international symposium on applications of computers and operations research in the mineral industries (APCOM)*, Cape Town (pp. 14–16).

Rossi, M. E., & Deutsch, C. V. (2014). *Mineral resource estimation*. Berlin: Springer.

Sadeghi, B., Madani, N., & Carranza, E. J. M. (2015). Combination of geostatistical simulation and fractal modeling for mineral resource classification. *Journal of Geochemical Exploration, 149,* 59–73.

Silva, D., & Boisvert, J. (2014). Mineral resource classification: A comparison of new and existing techniques. *Journal of the Southern African Institute of Mining and Metallurgy, 114,* 265–273.

Sinclair, A. J., & Blackwell, G. H. (2002). *Applied mineral inventory estimation*. Cambridge: Cambridge University Press.

Snowden, D. V. (2001). Practical interpretation of mineral resource and ore reserve classification guidelines. In A. C. Edwards (Ed.), Mineral resource and ore reserve estimation—The AusIMM guide to good practice: The Australasian Institute of Mining and Metallurgy, Monograph 23, Melbourne (p. 643–652).

Vallée, M. (1999). Resource/reserve inventories: What are the objectives? *CIM Bulletin, 92*(1031), 151–155.

Vallée, M. (2000). Mineral resource + engineering, economic and legal feasibility = ore reserve. *CIM Bulletin, 93*(1039), 53–61.

Wackernagel, H. (2003). *Multivariate geostatistics: An introduction with applications* (p. 387). Berlin: Springer.

Wackernagel, H. (2013). *Multivariate geostatistics: An introduction with applications*. Berlin: Springer.

Wawruch, T. M., & Betzhold, J. F. (2005). Mineral resource classification through conditional simulation. In *Geostatistics Banff 2004* (pp. 479–489). Springer.

Wilde, B. (2010). Programs for data spacing, uncertainty, and classification. CCG annual report 12, paper 403.

Yamamoto, J. K. (2000). An alternative measure of the reliability of ordinary kriging estimates. *Mathematical Geology, 32*(4), 489–509.